

# *Coupled versus uncoupled hindcast simulations of the Madden-Julian oscillation in the Year of Tropical Convection*

Article

Published Version

Shelly, A., Xavier, P., Copsey, D., Johns, T., Rodríguez, J. M., Milton, S. and Klingaman, N. (2014) Coupled versus uncoupled hindcast simulations of the Madden-Julian oscillation in the Year of Tropical Convection. *Geophysical Research Letters*, 41 (15). pp. 5670-5677. ISSN 0094-8276 doi: <https://doi.org/10.1002/2013GL059062> Available at <https://centaur.reading.ac.uk/37252/>

It is advisable to refer to the publisher's version if you intend to cite from the work. See [Guidance on citing](#).

To link to this article DOI: <http://dx.doi.org/10.1002/2013GL059062>

Publisher: American Geophysical Union

All outputs in CentAUR are protected by Intellectual Property Rights law, including copyright law. Copyright and IPR is retained by the creators or other copyright holders. Terms and conditions for use of this material are defined in the [End User Agreement](#).

[www.reading.ac.uk/centaur](http://www.reading.ac.uk/centaur)

**CentAUR**

Central Archive at the University of Reading

Reading's research outputs online

## RESEARCH LETTER

10.1002/2013GL059062

## Key Point:

- A dynamical interactive ocean improves MJO forecasts

## Supporting Information:

- Readme
- Figure S1

## Correspondence to:

A. Shelly,  
Ann.shelly@metoffice.gov.uk

## Citation:

Shelly, A., P. Xavier, D. Copsey, T. Johns, J. M. Rodríguez, S. Milton, and N. Klingaman (2014), Coupled versus uncoupled hindcast simulations of the Madden-Julian Oscillation in the Year of Tropical Convection, *Geophys. Res. Lett.*, *41*, 5670–5677, doi:10.1002/2013GL059062.

Received 26 JUN 2014

Accepted 27 JUL 2014

Accepted article online 31 JUL 2014

Published online 8 AUG 2014

## Coupled versus uncoupled hindcast simulations of the Madden-Julian Oscillation in the Year of Tropical Convection

Ann Shelly<sup>1</sup>, Prince Xavier<sup>1</sup>, Dan Copsey<sup>1</sup>, Tim Johns<sup>1</sup>, José M. Rodríguez<sup>1</sup>, Sean Milton<sup>1</sup>, and Nicholas Klingaman<sup>2</sup>

<sup>1</sup>Met Office, Exeter, UK, <sup>2</sup>Department of Meteorology, University of Reading, Reading, UK

**Abstract** This study investigates the impact of a full interactive ocean on daily initialized 15 day hindcasts of the Madden-Julian Oscillation (MJO), measured against a Met Office Unified Model atmosphere control simulation (atmospheric general circulation model (AGCM)) during a 3 month period of the Year of Tropical Convection. Results indicate that the coupled configuration (coupled general circulation model (CGCM)) extends MJO predictability over that of the AGCM, by up to 3–5 days. Propagation is improved in the CGCM, which we partly attribute to a more realistic phase relationship between sea surface temperature (SST) and convection. In addition, the CGCM demonstrates skill in representing downwelling oceanic Kelvin and Rossby waves which warm SSTs along their trajectory, with the potential to feedback on the atmosphere. These results imply that an ocean model capable of simulating internal ocean waves may be required to capture the full effect of air-sea coupling for the MJO.

### 1. Introduction

The Madden-Julian Oscillation (MJO) [Madden and Julian, 1971] is the leading mode of intraseasonal variability in the tropics. It exerts considerable influence on tropical weather and climate variability, such as the Indian and Asian monsoons [Goswami, 2005; Hsu, 2005; Wheeler and McBride, 2005] and tropical cyclone activity [Vitart, 2009], and can modulate extratropical weather patterns through forcing of atmospheric Rossby waves by the divergent outflow from tropical convection which propagate toward the midlatitudes [Ferranti et al., 1990; Cassou, 2008].

It has been demonstrated the forecast skill of MJO improves in atmospheric simulations if forced with high temporal frequency sea surface temperature (SST) variability and such simulations also display better rainfall variability [Klingaman et al., 2008; Matthews, 2004]. The importance of two-way interaction between atmosphere and ocean components in models [Woolnough et al., 2007; Fu et al., 2013] has also been suggested. Another potentially important aspect in successfully simulating the MJO in models is maintaining a correct phase relationship in the atmospheric response to SST anomalies [Kim et al., 2010; Fu et al., 2007].

Evidence is increasing that suggests ocean models may be necessary to capture dynamical ocean feedbacks important for initializing and maintaining the MJO. Webber et al. [2010, 2012] highlight the important role of ocean dynamics particularly in the Indian Ocean, where a tropical ocean internal wave response to the MJO leads to SST anomalies with the potential to feedback on the atmosphere and trigger further MJO events. Anomalous easterlies in the equatorial Indian Ocean can act to force a westward propagating downwelling (upwelling) Rossby wave, and SST increases (decreases) in phase with the passage of the wave [Seiki et al., 2013; Shinoda et al., 2013]. Drushka et al. [2012] demonstrate that mixed layer depth variations on MJO time scales modulate the heat budget by ~40% in the warm pool region. These studies imply that to accurately model the MJO, ocean dynamics may need to be simulated adequately enough to resolve internal waves as well as SST anomalies forced by waves. Developing a better picture for how MJO forcing impacts the ocean, and how this may feedback onto the MJO, is necessary for improving MJO prediction and modeling.

This study extends previous work by carrying out daily initialized MJO simulations with a global coupled Met Office Unified Model (MetUM) configuration and by using a more complex ocean model than has been previously applied to MJO and air-sea interactions investigations on medium range time scales. The experimental setup, outlined in section 2, permits us to examine the influence of the subsurface ocean on MJO simulations. As MetUM uncoupled operational forecast models already have a good general representation of the MJO on these time scales [Gottschalck et al., 2010], we consider the model a suitable

tool for analyzing the impact of two-way air-sea coupling on mechanisms instrumental in the lifecycle and predictability of the MJO.

## 2. Data and Methods

We compare MetUM models for a set of daily initialized 15 day hindcasts with observation and analysis data, for the period falling within the Year of Tropical Convection (YOTC). Two strong MJO episodes denoted as YOTCE (15 October to 6 December 2009) and YOTCF (16 December 2009 to 29 January 2010) with reference to Figure 3 of *Waliser et al.* [2012] form the central focus for our analysis.

The models used are a MetUM coupled general circulation model (CGCM) and a corresponding atmospheric general circulation model (AGCM) with prescribed ocean boundary conditions using persisted SST anomalies. Anomalies in the MetUM analysis are calculated relative to Hadley Centre sea ice and sea surface temperature data set climatology [*Rayner et al.*, 2003]. The anomaly is added to the evolving climatological cycle of SST on a daily basis to obtain the AGCM SST forcing. We persist SST anomalies instead of persisting initial SSTs as the seasonal cycle affects the amplitude of SSTs within a few days, indicated by sensitivity tests carried out at the Met Office.

The atmospheric model physics is based on the GlobalAtmos3.0 version [*Walters et al.*, 2011], at a resolution of 60 km in the horizontal with 85 vertical levels. The ocean component is based on Nucleus for European Modelling of the Ocean (NEMO) configured with version 3.2 physics on a  $0.25^\circ$  horizontal grid, with 75 vertical levels and 1 m vertical resolution in the top 10 m, coupled to The Los Alamos sea ice model. The atmosphere is initialized from MetUM analyses, the ocean component is initialized from NEMO Variational data assimilation system analyses [*Mogensen et al.*, 2009], and the models communicate on a 3 hourly coupling frequency. Any difference in hindcast skill in the CGCM compared to AGCM measures the impact of two-way air-sea interaction between the model components in dynamically predicting SSTs.

In order to measure MetUM performance and ability to represent processes key to the MJO, a number of metrics are calculated. This study focuses on dates which contain an MJO in the initial conditions; it does not include hindcasts from prior to the start of the MJO events. RMM1 and RMM2 are formed following the Wheeler and Hendon [*Wheeler and Hendon*, 2004, hereinafter WH] method, removing the annual mean and the first three harmonics of the annual cycle. Anomalies of Outgoing Longwave Radiation (OLR) and winds at 850 hPa ( $u_{850}$ ) and 200 hPa ( $u_{200}$ ) are combined and projected onto WH empirical orthogonal functions to yield real-time multivariate time series RMM1 and RMM2. Anomaly correlations are calculated against MetUM operational analysis following the method of *Gottschalck et al.* [2010] as a measure of MJO predictability in both model configurations. Significance of the correlation coefficients is tested using the Pearson critical value table. The sample sizes for YOTCE and YOTCF are 50 and 44, respectively.

We are interested in relationships which exist between the atmosphere and ocean, and the method of time-lagged correlations is used to examine the forcing of the atmosphere by the ocean and vice versa. The model data were regridded to a  $2.5^\circ \times 2.5^\circ$  grid, to match NOAA OLR observations. A band-pass filter is commonly used to isolate the MJO-related signal between 30 and 80 days in longer simulations, but it is not possible to apply this technique to 15 day hindcasts as the band-pass length exceeds hindcast length. Instead, to minimize high-frequency variability prior to calculating lagged relationships, a 5 day running mean is applied to the data. Either side of each 15 day hindcast is padded with MetUM analyses data, a viable technique at the beginning of the hindcast when model fields are close to initial conditions, but we acknowledge that the end of the hindcast will likely erroneously improve due to influence of the analysis. Therefore, we disregard hindcast data past day 13 that have been treated in this manner. This smoothing has only been applied to data used in Figure 2.

The lagged phase relationship between SST and convection is calculated, using OLR as a proxy for convection. A single 15 day initialized hindcast does not provide a sufficiently long time series to adequately assess lagged relationships. To circumvent this issue, we collect all of the day 5 lead times from each 15 day hindcast over the YOTCE and (separately) YOTCF period. We extract the Indian Ocean region from the full global data set and average over latitudes between  $10^\circ\text{N}$  and  $10^\circ\text{S}$ , for each point of longitude between  $60^\circ\text{E}$  and  $100^\circ\text{E}$  between the SST and OLR data sets. We subsequently perform lagged correlations between the data sets for lags of up to 15 days. At each longitude, the latitude-averaged OLR is lag correlated with the latitude-averaged SST, for leads and lags up to 15 days. NOAA OLR [*Liebmann and Smith*, 1996] observations

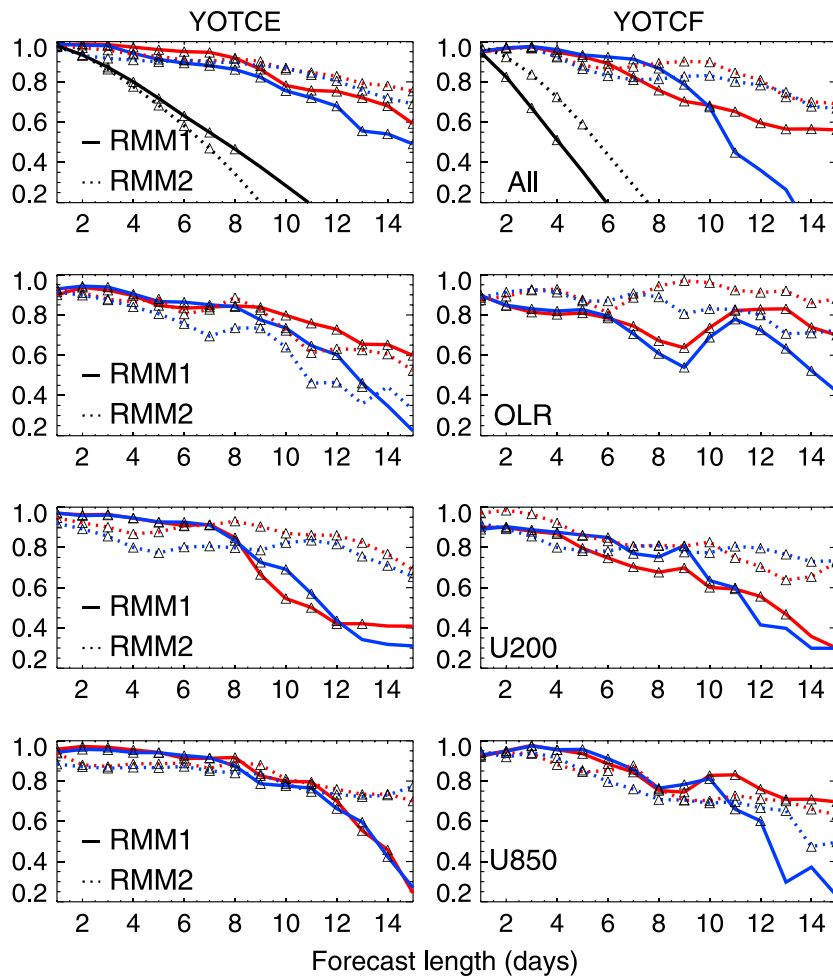


**Figure 1.** Hindcast anomaly correlation scores during (left) YOTCE and (right) YOTCF for (row 1) combined fields, (row 2) OLR, (row 3) U200, and (row 4) U850 as measured against MetUM analyses, for MJO amplitudes exceeding 1. All phases are included in each plot. The CGCM is in red and AGCM in blue. A persistence hindcast (black) is shown for combined fields. Significance at 99% level is denoted by a triangle.

and operational sea surface temperature and sea ice analyses (OSTIA) [Donlon *et al.*, 2012] are used to verify the data. Previous work [Klingaman *et al.*, 2011] suggests that correlations between these fields peak at a 10 day lag (see Figure S1 in the supporting information). In order to examine propagation of each YOTC event, we additionally calculate lagged correlations of OLR at a base point (70°E) with latitude-averaged OLR at all points of longitude in the Indian Ocean.

Chelton *et al.* [2003] demonstrated that Rossby waves generally have a sea surface height (SSH) maxima centered 40° of latitude away from the equator, with positive (negative) SSH anomalies associated with a downwelling (upwelling) Rossby wave. To assess the modeled representation of tropical ocean waves associated with the MJO, we examine anomalies of both SSH and depth of the 20°C isotherm (Dep20) and verify against daily Forecast Ocean Assimilation Model (FOAM) analyses [Storkey *et al.*, 2010] for these quantities. We validated the daily SSH FOAM analysis against Archiving Validation and Interpretation of Satellite Oceanographic data observations and these largely agree (not shown). To search for propagating Rossby waves, we form a latitudinal average between 2°N–8°N and 2°S–8°S in the Indian Ocean and plot time-longitude diagrams for the period spanning September 2009 to January 2010 for analyses and CGCM hindcasts at day 1 and day 14. To study equatorial Kelvin wave propagation, a latitudinal average is formed over the equatorial waveguide between 2°N and 2°S in the Indian Ocean.

### 3. Results

During YOTCE, the CGCM demonstrates enhanced performance for RMM1 over that of the AGCM from day 4 for combined fields, extending predictability by 3 days based on a threshold of 0.6 (Figure 1, left). The configurations display similar skill out to day 11 for RMM2, after which the CGCM is slightly more skillful. The persistence hindcast is shown to rapidly diverge from the dynamical hindcasts at day 1, indicating a rapid loss of predictability. Over YOTCF, the AGCM has greater RMM1 predictability from day 5 out to day 10, after which the score rapidly deteriorates. CGCM anomalies remain above a correlation of 0.6 in these later lead times (Figure 1, right) and extend predictability by 5 days in the case of RMM1 for combined fields based on a threshold of 0.6. However, both configurations are similar in the case of RMM2.

CGCM correlation scores for OLR are demonstrably better than the AGCM for both RMM1 and RMM2. Over the YOTCE period, the CGCM shows greater performance from day 8 (RMM1) and from day 4 (RMM2) and similarly for the YOTCF event, from day 6 (RMM1) to day 8 (RMM2). Performance is comparable for upper level winds as the two configurations remain close throughout lead times. Nonetheless, the CGCM displays a slight improvement over YOTCE, particularly for RMM2 and for RMM1 between days 12 and 15. In the case of U850, the CGCM shows generally greater predictability in the latter 5 days for YOTCF but similar performance over YOTCE. In general, the CGCM has greater predictability particularly for OLR and U850 and is capable of maintaining higher correlation scores over the entire hindcast length. The results for both simulations are found to be mostly significantly different from zero (denoted as triangles in Figure 1), but the differences between the two simulations are not found to be significant. We acknowledge that the study is somewhat limited by focusing on deterministic hindcasts of two MJO events and would expect some variation in evolution and characteristics between MJO events.

We next examine possible mechanisms leading to the improved predictability seen in the CGCM hindcasts. Propagation of the convective center of action of the MJO through the Indian Ocean over YOTCE is illustrated in Figures 2a–2c. The eastward propagation of the MJO is apparent in the observations throughout the period (Figure 2a). As the main center of convection follows a trajectory across the Indian Ocean and clear skies (positive OLR) turn cloudy (negative OLR), the correlations switch sign from negative to positive. The AGCM-simulated MJO is stationary by day 5 (Figure 2c). Lead-lag correlations as shown in Figure 2b for day 5, but constructed using respectively later days in the hindcast, indicate that the CGCM is still able to propagate the MJO out to day 9 hindcasts, though slower than observed (not shown). This result indicates that dynamically evolving SSTs play a role in improving propagation of the MJO and is corroborated by other studies [Fu *et al.*, 2007; Waliser *et al.*, 1999].

The lack of propagation of the MJO in the AGCM after a few days could be related to a loss of coherent evolution between atmospheric convection and underlying SST anomalies related to the MJO [Waliser *et al.*, 1999; Klingaman *et al.*, 2011]. In Figures 2d–2f, the SST-convection relationship is investigated through calculation of the lagged correlation between OLR and SST anomalies. Figures 2e and 2f depict the lagged correlation coefficients in the Indian Ocean for all day 5 hindcasts for the CGCM and AGCM for YOTCE. Similar results are obtained for YOTCF and in the Western Pacific (not shown). Observed warm SSTs are shown to lead enhanced convection by 5–10 days, and conversely, active convection leads cool SSTs by 5–10 days (Figure 2d). The CGCM reproduces the observed phase relationship, though it is slightly weaker and maintains the relationship out to day 13 lead time (not shown). However, in the AGCM experiment, convection adjusts to a location where SST anomalies peak, which results in colocated OLR and SST anomalies by day 5. In reality, warm SST anomalies not only influence the convection but are concurrently influenced by the atmospheric state. The AGCM is unable to reproduce this key air-sea interaction, and the MJO simulation suffers. A phase relationship analysis of operational global MetUM and climate model configurations is presented in the supporting information which corroborates results presented here.

Fu *et al.* [2013] found that an AGCM forced by daily observed SSTs can sustain the SST-convection relationship and that the match between the atmospheric MJO conditions and underlying SST is the important factor. However, this is not practical from an operational forecasting standpoint when the future evolution of the SST is unknown. Thus, the only way that this mechanism can be represented to the advantage of operational forecasting is through an interactive ocean.

It is clear from Figure 2 that that SST modulates and is modulated by the MJO. We next consider the CGCM representation of tropical ocean waves, which play a role in modulating the SST in the tropical warm pool

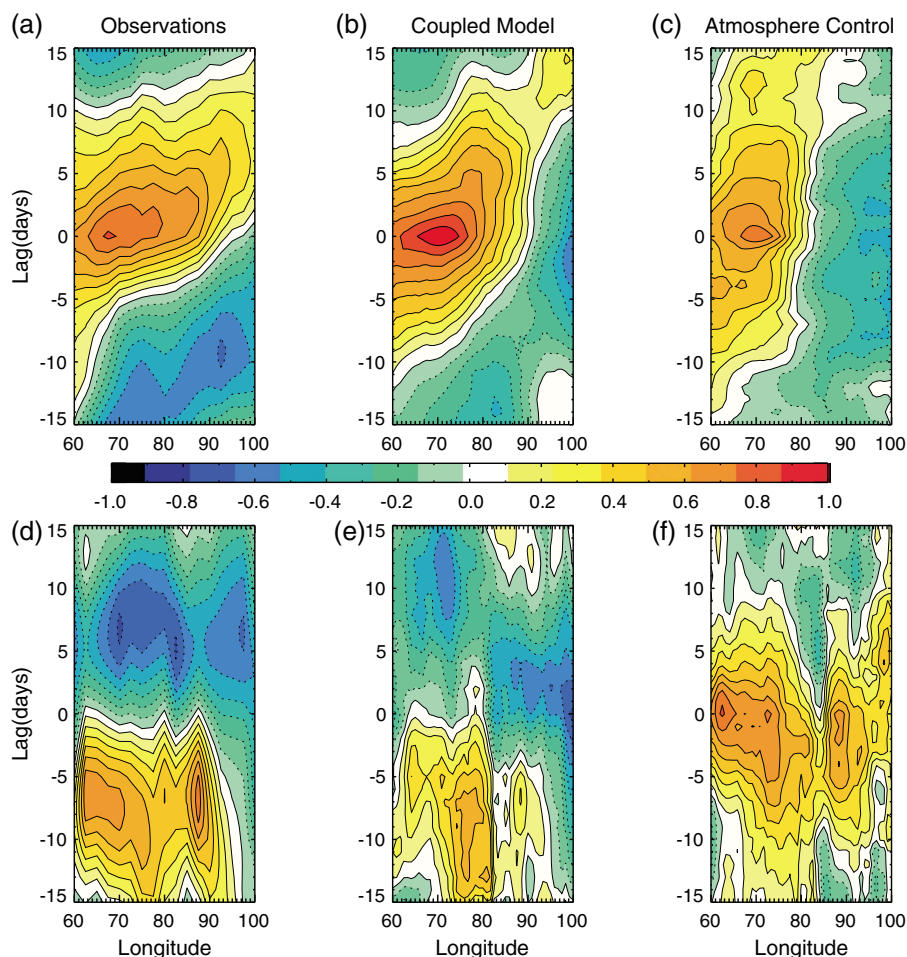


**Figure 2.** Lead-lag correlations for OLR at a base point of 70°E with OLR at all points of longitude in the Indian Ocean over YOTCE period (15 October to 6 December 2009) for (a) observations (b) CGCM, and (c) AGCM, for all day 5 hindcasts. Lead-lag correlations over YOTCE period (15 October to 6 December 2009) for SST correlated with OLR in the Indian Ocean for (d) observations, (e) CGCM hindcast, and (f) AGCM hindcast (surface temperature at sea points), for all day 5 hindcasts.

[Mccreary, 1983; Shinoda, 2005]. Downwelling waves deepen the thermocline and raise the SST by reducing entrainment of cold subsurface waters, while upwelling waves lead to enhanced entrainments and cooling. Suryachandra et al. [2012] demonstrate through a budget analysis that advection plays a key role in warming SSTs in the region, suggesting that it is important that tropical waves are well simulated in a GCM.

Enhanced convection and strong surface winds likely associated with the MJO YOTCE activity in mid-October excites an oceanic Kelvin wave which propagates eastward along the equator (Figure 3a) reaching the Maritime Continent in late November, visible as a positive anomaly moving eastward in the FOAM analysis Dep20 field. The perturbation in the ocean height (equatorial SSH, not shown) and at the thermocline (Dep20) is well reproduced in CGCM day 1 and day 14 hindcasts, with a propagation speed and amplitude similar to the FOAM analysis (Figures 3b and 3c). The modeled OLR is similar to observed OLR anomalies at day 1 (Figure 3b, contours) in magnitude and propagation but appears stationary by day 14 (Figure 3c).

Several westward propagating, downwelling Rossby waves are noticeable over the period between October 2009 and January 2010 (R1–R3). R1 propagates west from 65°E between September and early November (Figure 3d), R2 moves from 90°E to 60°E between September and January. The third observed wave (R3) is triggered in late November coinciding with YOTCE MJO propagation into the Maritime Continent and moves West from early December toward 80°E by mid-January. A potential mechanism for the trigger of R3 could

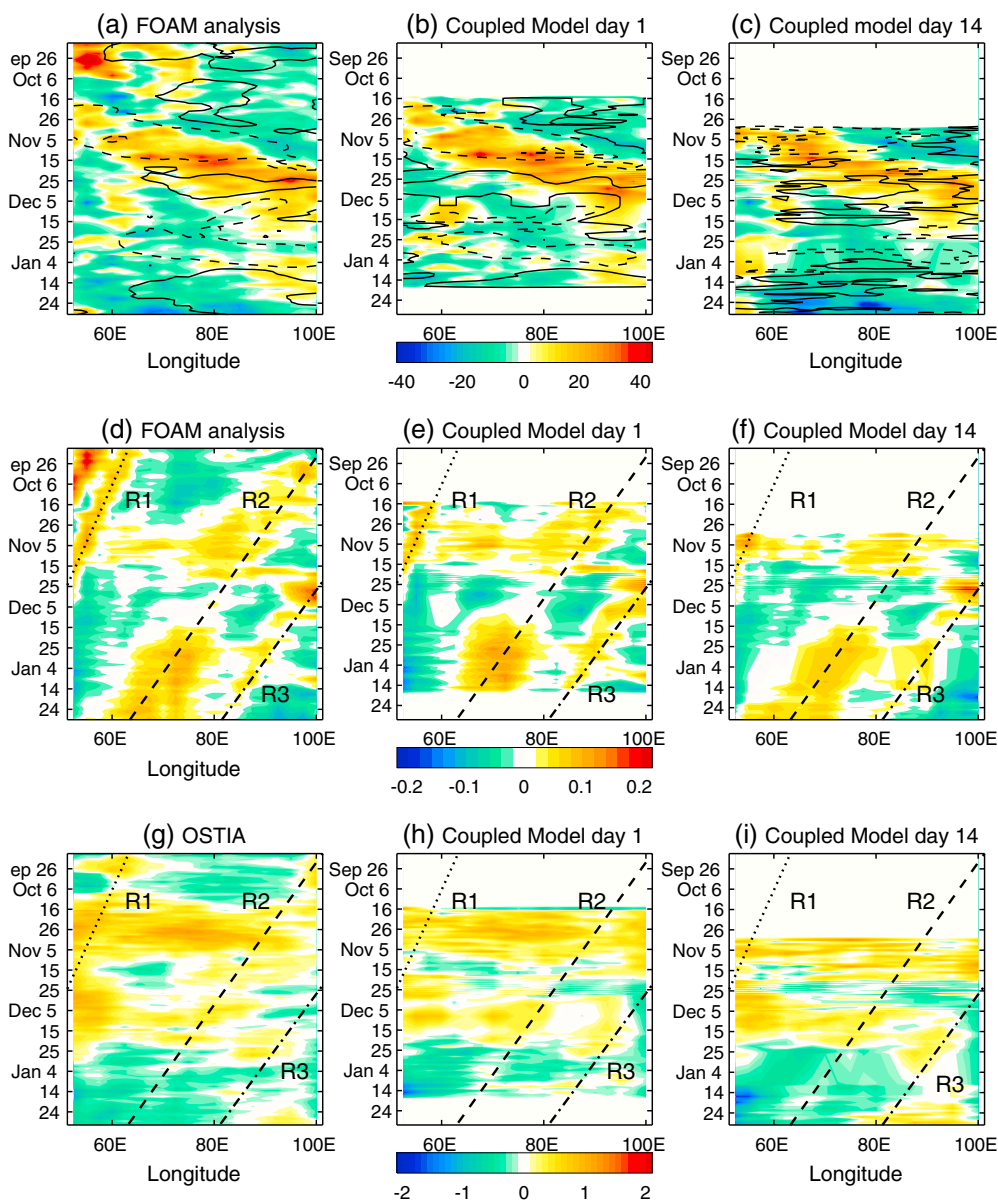


**Figure 3.** Time-longitude plots for (top) Dep20 anomaly (m) and OLR anomaly ( $\pm 10 \text{ W m}^{-2}$ ) for (a) FOAM analysis (shading) and NOAA OLR (contours), (b) day 1 CGCM hindcasts, and (c) day 14 CGCM hindcasts averaged between  $2^\circ\text{N}$  and  $2^\circ\text{S}$ ; (middle) SSH anomaly (m) for (d) FOAM analysis, (e) day 1 CGCM hindcasts, and (f) day 14 CGCM hindcasts averaged between  $2^\circ\text{N}$ – $8^\circ\text{N}$  and  $2^\circ\text{S}$ – $8^\circ\text{S}$ ; (bottom) SST anomaly field for (g) OSTIA, (h) day 1 CGCM hindcasts, and (i) day 14 CGCM hindcasts averaged between  $2^\circ\text{N}$ – $8^\circ\text{N}$  and  $2^\circ\text{S}$ – $8^\circ\text{S}$ . Diagonal lines (R1, R2, and R3) in Figures 3d–3i represent downwelling Rossby waves propagating from East to West across the Indian Ocean.

be through reflection and splitting of the earlier Kelvin wave back into the Indian Ocean along the Rossby waveguide at  $4^\circ\text{N/S}$  [Chelton *et al.*, 2003].

Though SST is sensitive to many processes and the daily SST anomaly field will contain high-frequency variability caused by surface fluxes and the diurnal cycle, there are clearly some westward propagating SST anomalies which follow the trajectory of the westward propagating Rossby waves (Figure 3g). The R1 wave seen in the SSH propagates westward at the same speed and direction as a warm SST anomaly seen in the OSTIA dataset (Figure 3g). It is possible that this wave could have had warmed SSTs prior to YOTCE, creating conditions more amenable to large-scale convection. Competing processes clearly play a role, and the prominent SST cooling caused by the passage of the YOTCE and YOTCF events is visible in the anomalously



cool conditions in mid-November and again in late December. Warming induced by the passage of R2 is likely overshadowed by entrainment of deeper, cooler waters brought about by strong winds and large-scale convection associated with the MJO event moving through the Indian Ocean. However, it does appear that there is westward propagation of positive SST anomalies superimposed on top of this pattern (Figure 3g). This is particularly obvious as a break in the eastward propagation of cool SST anomalies between 15 and 25 November, where the anomalies briefly turn slightly positive for about 10 days. Again, in the case of R3, there is an indication of westward motion of warm SSTs. The CGCM captures all three Rossby waves, and the SST anomaly fields largely resemble the OSTIA analysis. The influence of data assimilation is likely to be large on the initial days of the hindcast (Figure 3h); however, SSH and SST anomalies for day 14 hindcasts still retain resemblance to the analyses (Figures 3f and 3i). Warm SSTs advected by the tropical waves could potentially act as a positive feedback onto further convective events. *Webber et al.* [2012] showed that MJO events can coincide with the arrival of a downwelling oceanic equatorial Rossby wave in the western Indian Ocean, implying that such waves could act as a trigger.

#### 4. Conclusions

Our findings indicate that an interactive ocean produces improved MJO hindcasts over those of an AGCM forced with persisted SST anomalies. It is clear that there is potential for SST anomalies to be a key component of the MJO. Skill measures are improved in the CGCM likely because of the dynamical prediction of SSTs. We have not considered the complex impact of drift in the mean state of the CGCM on MJO hindcasts here, as SSTs in the Indian Ocean display minimal drift by day 14 over YOTCE/F (not shown). *Klingaman and Woolnough* [2014] address the separation of climate mean state influence on MJO simulation from improvements due to coupled processes in the Met Office Hadley Centre model, and we will address contributions from SST drifts on numerical weather prediction time scales in future work. We have demonstrated that the propagation of the MJO suffers in the AGCM simulation, which could result from the failure to represent the phase relationship that exists between convection and SST. The CGCM shows skill in representation of both oceanic equatorial Kelvin waves and of westward propagating Rossby waves out to 15 days. It has also been shown that while SST is sensitive to many different processes, anomalously warm waters occur along the trajectory of downwelling tropical waves, and this process could be important to the life cycle of the MJO. The case for using an ocean model capable of simulating waves seems strong, given that tropical waves appear both to influence and be influenced by the MJO.

#### Acknowledgments

The authors wish to thank Pat Hyder for useful advice and two anonymous reviewers for their constructive comments which have helped to improve this work. This work is supported by the Joint DECC/DEFRA Met Office Hadley Centre Climate Programme (GA01101). Data used to generate figures are available via contacting the lead author.

The Editor thanks two anonymous reviewers for their assistance in evaluating this paper.

#### References

- Cassou, C. (2008), Intraseasonal interaction between the Madden-Julian Oscillation and the North Atlantic Oscillation, *Nature*, 455(7212), 523–527.
- Chelton, D., M. Schlax, J. Lyman, and G. Johnson (2003), Equatorially trapped Rossby waves in the presence of meridionally sheared baroclinic flow in the Pacific Ocean, *Prog. Oceanogr.*, 56(2), 323–380.
- Donlon, C. J., M. Martin, J. Stark, J. Roberts-Jones, E. Fiedler, and W. Wimmer (2012), The operational sea surface temperature and sea ice analysis (OSTIA) system, *Remote Sens. Environ.*, 116, 140–158.
- Drushka, K., J. Sprintall, S. T. Gille, and S. Wijffels (2012), In situ observations of Madden-Julian Oscillation mixed layer dynamics in the Indian and western Pacific Oceans, *J. Clim.*, 25(7), 2306–2328.
- Ferranti, L., T. Palmer, F. Molteni, and E. Klinker (1990), Tropical extratropical interaction associated with the 30–60 day oscillation and its impact on medium and extended range prediction, *J. Atmos. Sci.*, 47(18), 2177–2199.
- Fu, X., B. Wang, D. E. Waliser, and L. Tao (2007), Impact of atmosphere-ocean coupling on the predictability of monsoon intraseasonal oscillations, *J. Atmos. Sci.*, 64(1), 157–174.
- Fu, X., J.-Y. Lee, P.-C. Hsu, H. Taniguchi, B. Wang, W. Wang, and S. Weaver (2013), Multi-model MJO forecasting during DYNAMO/CINDY period, *Clim. Dyn.*, 41(3–4), 1067–1081.
- Goswami, B. (2005), South Asian Monsoon, in *Intraseasonal Variability in the Atmosphere-Ocean Climate System*, edited by K. Lau and D. Waliser, pp. 19–61, Springer, New York.
- Gottschalck, J., et al. (2010), A framework for assessing operational Madden-Julian Oscillation forecasts: A CLIVAR MJO Working Group Project, *Bull. Am. Meteorol. Soc.*, 91(9), 1247–1258.
- Hsu, H. (2005), East Asian Monsoon, in *Intraseasonal Variability in the Atmosphere-Ocean Climate System*, edited by W. K. M. Lau and D. E. Waliser, pp. 63–90, Springer, Berlin, Heidelberg, Germany.
- Kim, H.-M., C. D. Hoyos, P. J. Webster, and I.-S. Kang (2010), Ocean-atmosphere coupling and the boreal winter MJO, *Clim. Dyn.*, 35(5), 771–784.
- Klingaman, N., and S. Woolnough (2014), The role of air-sea coupling in the simulation of the Madden-Julian Oscillation in the Hadley Centre Model, *Q. J. R. Meteorol. Soc.*, doi:10.1002/qj.2295.
- Klingaman, N. P., P. M. Inness, H. Weller, and J. M. Slingo (2008), The importance of high-frequency sea surface temperature variability to the intraseasonal oscillation of Indian monsoon rainfall, *J. Clim.*, 21(23), 6119–6140.
- Klingaman, N. P., S. J. Woolnough, H. Weller, and J. M. Slingo (2011), The impact of finer-resolution air-sea coupling on the intraseasonal oscillation of the Indian monsoon, *J. Clim.*, 24(10), 2451–2468.
- Liebmann, B., and C. Smith (1996), Description of a complete (interpolated) outgoing longwave radiation dataset, *Bull. Am. Meteorol. Soc.*, 77, 1275–1277.

- Madden, R. A., and P. R. Julian (1971), Detection of a 40–50 day oscillation in the zonal wind in the tropical Pacific, *J. Atmos. Sci.*, *28*(5), 702–708.
- Matthews, A. (2004), Atmospheric response to observed intraseasonal tropical sea surface temperature anomalies, *Geophys. Res. Lett.*, *31*, L14107, doi:10.1029/2004GL020474.
- Mccreary, J. (1983), A model of tropical ocean atmosphere interaction, *Mon. Weather Rev.*, *111*(2), 370–387.
- Mogensen, K., M. Balmaseda, A. Weaver, M. Martin, and A. Vidard (2009), NEMOVAR: A variational data assimilation system for the NEMO ocean model, in *ECMWF Newsletter*, pp. 17–21, ECMWF, Reading, U. K.
- Rayner, N., D. Parker, E. Horton, C. Folland, L. Alexander, and D. Rowell (2003), Global analyses of sea surface temperature, sea ice, and night marine air temperature since the late nineteenth century, *J. Geophys. Res.*, *108*(D14), 4407, doi:10.1029/2002JD002670.
- Seiki, A., M. Katsumata, T. Horii, T. Hasegawa, K. J. Richards, K. Yoneyama, and R. Shirooka (2013), Abrupt cooling associated with the oceanic Rossby wave and lateral advection during CINDY2011, *J. Geophys. Res. Oceans*, *118*, 5523–5535, doi:10.1002/jgrc.20381.
- Shinoda, T. (2005), Impact of the diurnal cycle of solar radiation on intraseasonal SST variability in the western equatorial Pacific, *J. Clim.*, *18*(14), 5523–5535.
- Shinoda, T., T. Jensen, M. Flatau, and S. Chen (2013), Surface wind and upper-ocean variability associated with the Madden Julian Oscillation simulated by the Coupled Ocean Atmosphere Mesoscale Prediction System (COAMPS), *Mon. Weather Rev.*, *141*, 2290–2307.
- Storkey, D., E. W. Blockley, R. Furner, C. Guiavarc'h, D. Lea, M. J. Martin, R. M. Barciela, A. Hines, P. Hyder, and J. R. Siddorn (2010), Forecasting the ocean state using NEMO: The new FOAM system, *J. Oper. Ocean*, *3*(1), 3–15.
- Suryachandra, A., R. Dhakate, S. Saha, S. Mahapatra, H. Chaudhari, S. Pokhrel, and S. Sahu (2012), Why is Indian Ocean warming consistently?, *Clim. Change*, *110*(3–4), 709–719.
- Vitart, F. (2009), Impact of the Madden Julian Oscillation on tropical storms and risk of landfall in the ECMWF forecast system, *Geophys. Res. Lett.*, *36*, L15802, doi:10.1029/2009GL039089.
- Waliser, D., K. Lau, and J. Kim (1999), The influence of coupled sea surface temperatures on the Madden-Julian oscillation: A model perturbation experiment, *J. Atmos. Sci.*, *56*(3), 333–358.
- Waliser, D. E., et al. (2012), The year of tropical convection (May 2008–April 2010): Climate variability and weather highlights, *Bull. Am. Meteorol. Soc.*, *93*, 1189–1218.
- Walters, D. N., et al. (2011), The Met Office Unified Model Global Atmosphere 3.0/3.1 and JULES Global Land 3.0/3.1 configurations, *Geosci. Model Dev.*, *4*(4), 919–941.
- Webber, B. G. M., A. J. Matthews, and K. J. Heywood (2010), A dynamical ocean feedback mechanism for the Madden-Julian Oscillation, *Q. J. R. Meteorol. Soc.*, *136*, 740–754.
- Webber, B. G. M., A. J. Matthews, K. J. Heywood, and D. P. Stevens (2012), Ocean Rossby waves as a triggering mechanism for primary Madden-Julian events, *Q. J. R. Meteorol. Soc.*, *138*, 514–527.
- Wheeler, M., and H. Hendon (2004), An all-season real-time multivariate MJO index: Development of an index for monitoring and prediction, *Mon. Weather Rev.*, *132*(8), 1917–1932.
- Wheeler, M., and J. McBride (2005), Australian-Indonesian Monsoon, in *Intraseasonal Variability in the Atmosphere-Ocean Climate System*, pp. 125–168, Springer, Berlin, Heidelberg, Germany.
- Woolnough, S. J., F. Vitart, and M. A. Balmaseda (2007), The role of the ocean in the Madden-Julian Oscillation: Implications for MJO prediction, *Q. J. R. Meteorol. Soc.*, *133*, 117–128.